Anisotropic elastic properties of human femoral cortical bone and relationships with composition and microstructure in elderly

Article *in* Acta Biomaterialia · March 2019

DOI: 10.1016/j.actbio.2019.03.043

CITATIONS
0

READS
67

15 authors, including:

Xiran Cai
Stanford University
23 PUBLICATIONS **24** CITATIONS
SEE PROFILE

Hélène Follet
French Institute of Health and Medical Research
77 PUBLICATIONS **855** CITATIONS
SEE PROFILE

Laura Peralta
King's College London
52 PUBLICATIONS **68** CITATIONS
SEE PROFILE

Rémy Gauthier
Claude Bernard University Lyon 1 - INSA de Lyon
14 PUBLICATIONS **17** CITATIONS
SEE PROFILE

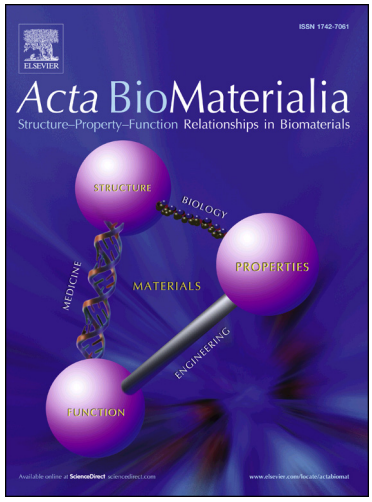

Anisotropic elastic properties of human femoral cortical bone and relationships with composition and microstructure in elderly

Xiran Cai, Hélène Follet, Laura Peralta, Marc Gardegaront, Delphine Farlay, Rémy Gauthier, Boliang Yu, Evelyne Gineyts, Cécile Olivier, Max Langer, Aurelien Gourrier, David Mitton, Françoise Peyrin, Quentin Grimal, Pascal Laugier

PII: S1742-7061(19)30218-1
DOI: https://doi.org/10.1016/j.actbio.2019.03.043
Reference: ACTBIO 6025

To appear in: *Acta Biomaterialia*

Received Date: 24 November 2018
Revised Date: 19 March 2019
Accepted Date: 20 March 2019

Please cite this article as: Cai, X., Follet, H., Peralta, L., Gardegaront, M., Farlay, D., Gauthier, R., Yu, B., Gineyts, E., Olivier, C., Langer, M., Gourrier, A., Mitton, D., Peyrin, F., Grimal, Q., Laugier, P., Anisotropic elastic properties of human femoral cortical bone and relationships with composition and microstructure in elderly, *Acta Biomaterialia* (2019), doi: https://doi.org/10.1016/j.actbio.2019.03.043

Anisotropic elastic properties of human femoral cortical bone and relationships with composition and microstructure in elderly

Xiran Cai[a,*], Hélène Follet[b], Laura Peralta[a], Marc Gardegaront[b], Delphine Farlay[b], Rémy Gauthier[c], Boliang Yu[d], Evelyne Gineyts[b], Cécile Olivier[d,e], Max Langer[d], Aurelien Gourrier[f], David Mitton[c], Françoise Peyrin[d,e], Quentin Grimal[a], Pascal Laugier[a]

[a] *Sorbonne Université, INSERM, CNRS, Laboratoire d'Imagerie Biomédicale (LIB), F-75006 Paris, France*
[b] *Univ Lyon, Université Claude Bernard Lyon 1, INSERM, LYOS UMR 1033, F-69008 Lyon, France*
[c] *Univ Lyon, Université Claude Bernard Lyon 1, IFSTTAR, LBMC UMR_T9406, F-69622 Lyon, France*
[d] *Univ Lyon, Université Claude Bernard Lyon 1, INSERM U1206, CNRS UMR 5220, INSA Lyon, CREATIS, F-69621 Villeurbanne Cedex, France*
[e] *ESRF, F-38043 Grenoble, France*
[f] *Univ Grenoble Alpes, CNRS, LIPhy, F-38000 Grenoble, France*

Abstract

The strong dependence between cortical bone elasticity at the millimetre-scale (mesoscale) and cortical porosity has been evidenced by previous studies. However, bone is an anisotropic composite material made by mineral, proteins and water assembled in a hierarchical structure. Whether the variations of structural and compositional properties of bone affect the different elastic coefficients at the mesoscale is not clear. Aiming to understand the relationships between bone elastic properties and compositions and microstructure, we applied state-of-the-art experimental modalities to assess these aspects of bone characteristics. All elastic coefficients (stiffness tensor of the transverse isotropic bone material), structure of the vascular pore network, collagen and mineral properties were measured in 52 specimens from the femoral diaphysis of 26 elderly donors. Statistical analyses and micromechanical modeling showed that vascular pore volume fraction and the degree of mineralization of bone are the most important determinants of cortical bone anisotropic mesoscopic elasticity. Though significant correlations were observed between collagen properties and elasticity, their effects in bone mesoscopic elasticity were minor in our data. This work also provides a unique set of data exhibiting a range of variations of compositional and microstructural cortical bone properties in the elderly and gives strong experimental evidence and basis for further development of biomechanical models for human cortical bone.

Keywords: Cortical bone, Elasticity, Microstructure, Composition, Resonant ultrasound spectroscopy

*Corresponding author
Email address: xirancai@stanford.edu (Xiran Cai)

1. Introduction

Human cortical bone is a porous composite material consisting of a soft organic matrix hardened by a mineral phase, composed of about 70% mineral (hydroxyapatite), 22% proteins (type I collagen) and 8% water by weight [1], assembled in a hierarchical structure that extends over several organization levels [2, 3]. At the nanoscale, the fibrils mainly constituted by collagen and hydroxyapatite are arranged in fibers. Mineralized fibers are organized to form bone lamellae whose typical thickness is about several micrometers. Across lamellar sublayers, the orientation of the fibers may vary and presents a twisted plywood structure [4]. At the microscale, the osteon, a cylindrical structure composed of several concentric lamellae around a Haversian canal ($20 - 100$ μm in diameter), constitutes the basic structural unit at this level. The cortical porosity includes the Haversian canals which are inter-connected by Volkmann's canals (several tens μm in diameter), osteocyte lacunae and canaliculi (a few μm to less than 1 μm in diameter) and resorption cavities. The pores mainly contain fluids and soft tissues, such as blood vessels, nerves and cells [5].

Bone undergoes a permanent biological remodeling process regulated by mechanosensitive osteocytes, which allows it to adapt to the mechanical load it sustains [6]. Osteocytes respond to the local strain, which, for a given load, is determined by bone stiffness. Hence investigating bone stiffness in detail should improve the understanding of bone functional adaptation mechanisms. The role of cortical bone as a determinant of bone strength and the role of cortical structural indices as a quantifiable marker of bone loss and bone fragility has been recognized recently [7]. In the femoral neck, cortical bone plays a predominant role compared to trabecular bone in respect to bone strength [8]. Even in the vertebral body, 45-75% of the axial load applied in compression is carried by the cortex [9]. Many case-control and cross-sectional studies have demonstrated that impaired cortical bone at the radius or tibia is associated with prevalent fractures of the wrist, hip or spine, even after adjustment for areal bone mineral density [10–13]. A few prospective studies recently indicated that deficit in cortical density and structure was predictive of incident fracture [14, 15]. All these results highlight the growing recognition of the role of cortical bone for the mechanical competence and of its deterioration as an important fracture risk. Cortical bone stiffness at the mesoscale (millimeter-scale) is of special interest as it has a direct impact on the mechanical behavior of bone at the macroscale level [6, 16] at which cortical bone acts, in concert with the overall gross shape of a bone, to resist functional loads [17]. The mesoscopic level is also appropriate to investigate the regional variations of the elastic properties within a bone [18], which is necessary to refine finite element models to predict patterns of stress and strain of major skeletal sites of osteoporotic fractures.

Bone mesoscopic stiffness depends on both the porous microstructure and the tissue

elastic properties at all the smaller lengthscales. Tissue elastic properties are determined by the composition and the structural organization of the tissue components. The inquiry of the role of composition and microstructure in the variation of bone stiffness dates back to the 70's [19, 20] when the importance of porosity and mineral content was identified.

Although vascular porosity has been found to be an important determinant of bone mesocale stiffness [19, 21, 22], the role of the three-dimensional (3-D) microstruture of the pore network in cortical bone stiffness is barely studied. Microstructural features, such as pore size, pore number, pore diameter, pore connectivity are footprints of the bone remodelling process [23] and may also have an effect on bone stiffness. A recent study has demonstrated that changes in pore network microstructure occurring during growth and aging may impact fibula cortical bone stiffness [24].

An important property of bone matrix is its mineral content which has been evaluated in various ways, including chemically dissolved [25] and burning up the organics in high temperature [26], and inferred by X-ray based methods [27, 28]. Depending on the evaluation methods different names have been used to describe the mineral content, such as calcium content, ash density, bone mineral density and degree of mineralization of bone (DMB). The Young's modulus of bone was found to be correlated with the calcium content [25] and the variability of the Young's modulus between children and adults' cortical bone can be largely explained by the ash density [26]. The recent advent of high resolution X-ray-based imaging modalities (e.g., microradiography, microcomputed tomography) allows accurate measurement of DMB and its spatial distribution. There is a lack, however, of studies to correlate the volumetric values with bone elasticity. Other compositional properties such as crystallinity which reflects the size and perfection of crystals, maturity of mineral and collagen, as well as collagen crosslinks are also a vital part of bone composition and are also associated with bone stiffness [29, 30], especially in diseases, such as osteogenesis imperfecta [31] or drug treated bone, e.g., by bisphosphonates [32, 33].

Although several studies investigating bone stiffness (i.e., elasticity) determinants have involved many microstructural and compositional (mineralization, crystallinity and collagen) features, bone was seldom considered as an anisotropic material and the relative contribution of these characteristics to bone anisotropic stiffness were not quantified. In this work, we carry out a thorough investigation of the determinants of cortical bone mesoscale anisotropic stiffness by applying state-of-the-art experimental modalities to assess the properties of the collagen and mineral, and the structure of the vascular pore network. To measure the anisotropic elastic properties, we use resonant ultrasound spectroscopy (RUS) which became recently available to measure bone and is, as far as we know, the most precise method to measure all elastic constants on small specimens. To measure the characteristics

of the vascular pores and mineral content, we use synchrotron radiation micro-computed tomography (SR-μCT) which is the reference technique for these purposes. To measure the amount of collagen and cross-links, we use a standard biochemistry method. To measure the properties of the mineral, we use a conventional Fourier transform infrared microspectroscopy technique (FTIRM). Combining all these techniques, the study provides a unique set of data exhibiting a range of variations of compositional and microstructural cortical bone properties. In addition to a thorough statistical analysis of the datasets, we interpret and summarize the observed trends of variations of elasticity resorting to a model based on micromechanics theory.

2. Materials and methods

2.1. Specimens

Bone specimens were harvested from the left femur of 29 human cadavers. The femurs were provided by the Département Universitaire d'Anatomie Rockefeller (French body donation to science program, declaration number: DC-2015-2357; Laboratory of Anatomy, Faculty of Medicine Lyon Est, University of Lyon, France) through the French program on voluntary corpse donation to science. Among the donors, 16 were females and 13 were males ($50-95$ years old, 77.8 ± 11.4, mean$\pm$SD). The fresh material was frozen and stored at $-20°$C. The samples were slowly thawed and then, for each femur, approximately a 40 mm-thick cross section was cut perpendicular to the bone axis from the mid-diaphysis. The cross section was separated to four sections corresponding to four quadrants (lateral, medial, anterior and posterior). In each of the lateral and medial anatomical quadrants, 3 rectangular parallelepiped shaped specimens (set #1, #2 and #3) were prepared along the axial direction for different testing purposes (Fig. 1). The elastic properties, the microstructural characteristics of the pore network and the degree of mineralization were obtained from set #1. Specimens #2 were prepared for mechanical testing aiming at estimating toughness. The results of mechanical testing have been reported in a separate publication [34]. The residues around the set #2 after cutting for #2 were used to assess collagen properties. Assessment of mineral properties was achieved using set #3. The nominal specimen size of set #1, #2 and #3 was $3\times4\times5$ mm^3, $3\times4\times25$ mm^3 and $3\times4\times0.5$ mm^3 in radial (axis 1), circumferential (axis 2) and axial direction (axis 3), respectively, defined by the anatomic shape of the femoral diaphysis. All specimens were kept hydrated during sample preparation.

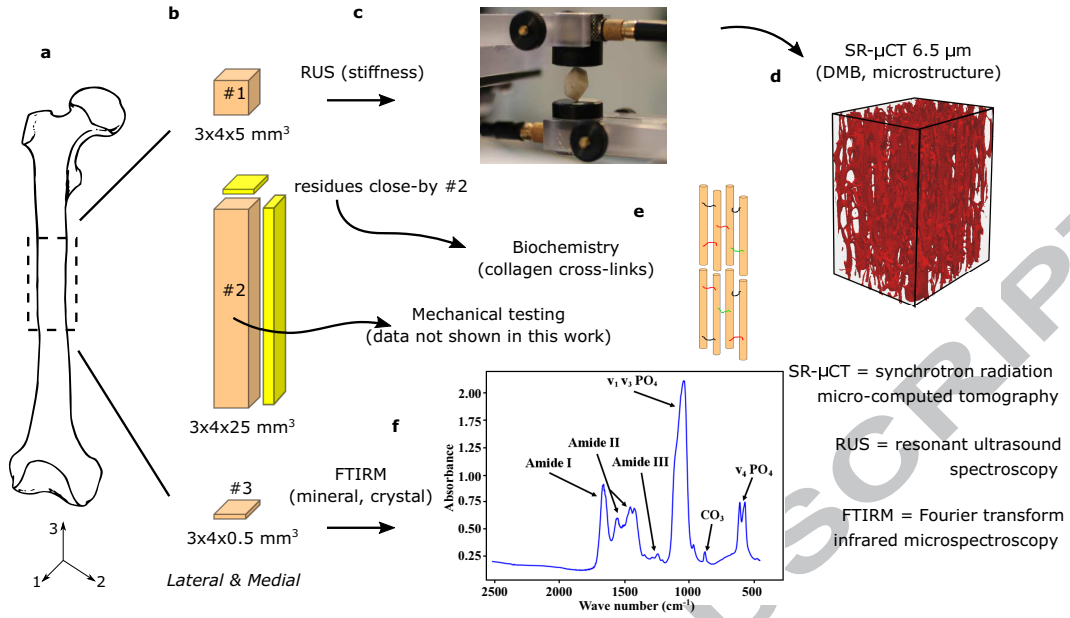

Figure 1: Sample preparation procedure and the representations of the experimental modalities including RUS, SR-μCT, biochemistry and FTIRM. (a) A cross-section of femoral bone at the mid-diaphysis was extracted. (b) Three rectangular parallelepiped shaped specimens (set #1, #2 and #3) were prepared along the axial direction at both the lateral and medial quadrants. (c) RUS measurements for bone stiffness. (d) Pore network obtained treating bone phase as background. (e) Bone residues around #2 after cutting for #2 went to biochemistry experiments to quantify the collagen and cross-links. (f) A FTIRM spectra containing compositional information of the bone specimen.

2.2. Bone stiffness measurements

The stiffness constants of bone specimens (set #1) were identified using RUS following the procedure previously described in Bernard et al. [35]. In RUS, the stiffness constants are estimated by solving an inverse problem which consists of the comparison of measured resonant frequencies to model-predicted frequencies (equation A.1). Briefly, the experiment consisted of the following steps: (1) A bone specimen was placed on two opposite corners between two ultrasonic shearwave transducers (V154RM, Panametrics, Waltham, MA), one for emission and one for reception, to achieve a free boundary condition for vibration. (2) The frequency response of the vibration of the specimen in the 100 - 600 kHz frequency bandwidth was amplified by a broadband charge amplifier (HQA-15 M-10 T, Femto Messtechnik GmbH, Berlin, Germany) and then recorded by a vector network analyzer (Bode 100, Omicron Electronics GmbH, Klaus, Austria), from which the 20 to 30 first resonant frequencies were extracted. (3) Assuming a transversely isotropic symmetry [36, 37] (plane 1-2 is the plane of isotropy), the stiffness constants C_{ij} (Voigt notation: $ij = 11; 33; 13; 44; 66$), were automatically calculated by optimizing the misfit function between the experimental and model predicted resonant frequencies (inverse problem), which was formulated in a Bayesian

framework [38]. The *prior* information of the distribution of the stiffness constants required for the Bayesian analysis was taken from a previous study [22].

In the elastic tensor, C_{11} and C_{33} which correspond to pure longitudinal waves are denoted as longitudinal stiffness constants; C_{44} and C_{66} which correspond to pure shear waves are denoted as shear stiffness constants; C_{12} and C_{13} are the off-diagonal stiffness constants corresponding to the mixed-mode waves [39]. For transverse isotropy, the following relations hold, $C_{11} = C_{22}$, $C_{44} = C_{55}$, $C_{13} = C_{23}$ and $C_{12} = C_{11} - 2C_{66}$. For transversely isotropic symmetry, the engineering moduli such as Young's moduli and Poisson's ratios can be converted by the stiffness tensor [5]. The mass density of each specimen, which is needed in stiffness determination with RUS, was derived from the average values of four mass (Sartorius CPA224s, precision: 0.1 mg) and dimensions measurements (Mitutoyo Coolant Proof Caliper 500-606, precision: 0.01 mm). The experimental errors caused by an irregularity of the specimen geometry and by uncertainties of the extracted resonant frequencies, following this protocol, typically cause an error of approximately 1.7% for the shear stiffness constants and approximately 3.1% for the compression and off-diagonal stiffness constants [40].

2.3. Bone microstructure

After RUS measurements, bone specimens in set #1 were defatted for 12 hours in a chemical bath of diethylether and methanol (1:1) and rinsed in distilled water before SR-μCT scanning in order to comply with the local regulation by the European Synchrotron Radiation Facility (ESRF, Grenoble, France). This defatting protocol does not alter the anisotropic stiffness of human cortical bone measured by RUS as has been verified in a previous work [41]. 3-D imaging acquisitions were performed on the beamline ID19 at ESRF using a SR-μCT setup based on a 3-D parallel beam geometry acquisition [42, 43]. We used a pink beam energy at 26 keV allowing fast image acquisition (0.2 s per projection) and a total acquisition time less than 10 min per scan. A full set of 2D radiographic images was recorded using a CDD detector (Gadox scintillator, optic lenses, 2048 $\times$ 2048 Frelon Camera) by rotating the specimen in 1999 steps within a 360° range of rotation. The detector system was fixed to get a pixel size of 6.5 μm in the recorded images in which a region of interest of 1400$\times$940 pixels was selected to fit the specimen. For each specimen, the SR-μCT 3-D volumes were reconstructed using a 3-D version of the Filtered Back Projection algorithm implemented at ESRF in the PyHST code [44].

In the reconstructed volume of each specimen, a volume of interest (VOI, sized approximately $2.8 \times 3.9 \times 4.8$ mm^3) was selected manually for morphometric analysis. Following [24], the VOIs were binarized by simple thresholding treating the void volumes as a solid and the bone phase as a background (Fig. 2). Then, the morphometric parameters listed in Table 1 were calculated using the software CTAn (V 1.16.1, Skyscan NV, Kontich, Belgium).

Table 1: Microstructure variables assessed by CTAn and their definitions.

Variable	Unit	Definition
Microstructure group		
ϕ	%	pore volume fraction
PoS/PoV	mm^{-1}	pore surface to pore volume ratio
PoN	mm^{-1}	pore number per millimeter
PoDm	μm	average diameter of the pores
PoSp	μm	average separation between pores
PoPf	mm^{-1}	pore pattern factor, lower PoPf indicates higher concavity, i.e., better-connected pore network
ConnD	mm^{-3}	connectivity density, a measure of the degree to which a pore is multiply connected
SMI	a.u.	structure model index, the relative prevalence of rods and plates in a 3D pore network

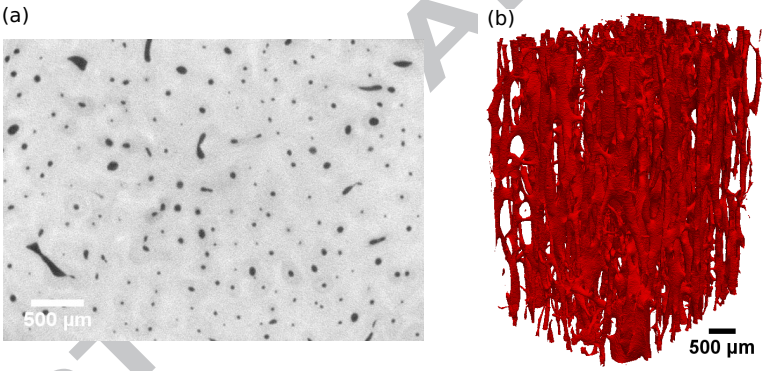

Figure 2: (a) One transverse gray-levels cross-section of cortical bone scanned by SR-μCT showing the distribution of pores and mineral. (b) 3-D rendering of the pore network after binarization of the volume.

2.4. Degree of mineralization of bone

A pink beam was used in the first SR-μCT experiments on the beamline ID 19 which did not provide satisfying values of degree of mineralization of bone (DMB). Hence, SR-μCT experiments were launched for a second time on the same specimens (set #1) on the beamline ID 17 at ESRF using a monochromatic beam. The beam energy was accurately tuned to 26.5 keV by using a Laue-Laue monochromator. The detector was a PCO edge CMOS camera coupled to a YAG scintillator. The pixel size was set to 6.03 μm and counting time was 0.4 s per projection. A total set of 4000 projections was acquired under 360° yielding to a total scan time of 30 min per sample. The 3-D volume were reconstructed using PyHST as previously described.

The gray levels of the images (Fig. 2), corresponding to the X-Ray linear absorption coefficients of bone, were used to estimate the 3D distribution of mineral content within a bone specimen as described in [45]. As the linear attenuation of collagen and water are very close [46, 47], we have considered only a two-material decomposition basis, made of hydroxyapatite and water. In addition, since we used a monochromatic synchrotron CT acquisition, the energy of the incoming X-ray beam is perfectly known. Then this allows the estimation of the mineral concentration (g/cm^3), namely DMB, from the measured linear attenuation coefficient as described in [45]. The DMB was averaged on the whole 3-D bone phase after taking care of partial volume effects.

2.5. Biochemical measurements

The spared materials from the preparation of specimens #2 were cut into small pieces, powdered, demineralized, extensively washed and hydrolyzed. The amount of enzymatic cross-links (DHLNL, HLNL, PYD and DPD), non-enzymatic cross-link pentosidine (PEN) (Table 2) and collagen were quantified using the hydrolysates. Detailed process of the biochemical experiments has been reported in Gauthier et al. [48]. The measurement error of the cross-links was evaluated previously in bovine bone which was between 5.2-10.7% [49, 50]. The variables from biochemical measurements are summarized in Table 2 grouped as collagen variables.

2.6. Fourier transform infrared microspectroscopy

FTIRM analysis is done on 2 μm thin sections. To do so, after dissection of bone, samples (set #3) were fixed in 70% ethanol for two weeks, dehydrated for 48h in 100% ethanol, substituted for 48h in methylcyclohexane and then embedded in methylmethacrylate (MMA). The sections of 2 μm thickness were obtained with a microtome Polycut E (Reichert-Jung, Leica, Germany) and stored between two slides at room temperature. The raw spectra were collected at 1 cm^{-1} resolution and averaged by 40 scans per scanned region in transmission mode with a Perkin–Elmer GXII Auto-image Microscope (Norwalk, CT, USA) equipped with a wide band detector (mercury-cadmium-telluride) (7800-400 cm^{-1}). The instrument used a Cassegrain objective of numerical aperture 0.6. The system has a spatial resolution of 10 μm at typical midinfrared wavelengths. Contribution from air was subtracted from original spectrum. The preprocessing (MMA removal, baseline correction) and the analysis by peak fitting were executed using the LYOS Spectrum Analysis software [51].

From the spectrum, the following variables (Table 2) were retrieved: mineral to matrix ratio (MinOrga) which represents the ratio of the mineral phase over the organic phase (collagenic and non-collagenic proteins), mineral maturity (MinMat) which reflects the transformation of non apatitic phosphates of the hydrated layer into apatitic phosphates contained

in the crystal core, carbonation (Carbon) which represents the quantity of carbonates incorporated into the bone mineral at a labile site and substituted in the apatite lattice due either to PO_4 or OH, crystallinity index (CryInd) which corresponds to both crystalline domain size and how well the ions of the crystal are ordered in the unit cells and collagen maturity (CollMat). The reproducibility of each FTIRM variable was calculated on human cortical bone section, with a region of interest 100 μm $\times$ 100 μm (spatial resolution), at 2 cm^{-1} spectral resolution. It was calculated as the standard deviation over mean of 10 measurements and was, for MinOrga (0.4%), MinMat (0.8%), Carbon (0.3%), CryInd (0.7%) and CollMat (5.6%). More details of the definition of these variables can be found in Table 2. The former four variables were grouped in the mineral variable group and the last one CollMat was grouped in the collagen variable group.

Table 2: Compositional variables assessed by FTIRM, SR-μCT and biochemistry experiments and their definitions.

Variable	Unit	Definition	Modality
Mineral group			
DMB	g/cm^3	Degree of mineralization of bone	SR-μCT
MinOrga	no unit	Mineral to matrix ratio, the ratio of the $\nu_1\nu_3PO_4$ area ($910 - 1184$ cm^{-1}) over the Amide I area ($1592 - 1730$ cm^{-1})	FTIRM
MinMat	no unit	Mineral maturity, the ratio of the apatitic ($\sim$1030 cm^{-1} peak) over non apatitic ($\sim$1110 cm^{-1} peak)	FTIRM
Carbon	no unit	Carbonation, the ratio of the ν_2CO_3 area ($862 - 894$ cm^{-1}) over the $\nu_1\nu_3PO_4$ area	FTIRM
CryInd	cm	Crystallinity index, the inverse of the full width FTIRM at half maximum of the $\sim$604 cm^{-1} peak	FTIRM
Collagen group			
CollMat	no unit	Collagen maturity, $\sim$1660 cm^{-1} peak over $\sim$1690 cm^{-1} peak	FTIRM
DHLNL	mmol/mol collagen	Didhydroxylysinonorleucine, immature enzymatic cross-links	Biochemistry
HLNL	mmol/mol collagen	Hydroxylysinonorleucine, immature enzymatic cross-links	Biochemistry
PYD	mmol/mol collagen	Pyridinoline, mature enzymatic cross-links	Biochemistry
DPD	mmol/mol collagen	Deoxypyridinoline, mature enzymatic cross-links	Biochemistry
PEN	mmol/mol collagen	Pentosidine, non-enzymatic cross-links	Biochemistry
Coll	%	Collagen percentage by weight	Biochemistry

2.7. Statistics

After calculating the descriptive statistics, a statistical analysis was conducted to exhibit empirical relationships between elasticity, on the one hand, and the variables in the microstructural, mineral and collagen groups, on the other hand. The mean value, standard deviation (SD) and coefficient of variation (CV), expressed as the ratio SD/Mean are reported for each variable. Normality of the distribution of the variables was evaluated using the Shapiro-Wilk test. One-way analysis of variance (ANOVA) and Wilcoxon test (for the variables failing the normality test) were performed to evaluate the differences of the data sets from lateral and medial anatomical quadrants. As some variables were not normally distributed, we used Spearman rank coefficients in the correlation analyses between stiffness constants and each of the microstructural and compositional variables. Those variables significantly correlated with at least one stiffness constant were kept for a series of stepwise multiple linear regression analyses. For each stiffness constant, stepwise analyses were firstly carried out in each group of variables (microstructure, mineral and collagen). Then, the most significant variables of each group were retained to find the optimal multiple linear regression model. For those variables for which we observed a difference between lateral and medial quadrants, the multiple linear regression analyses were carried out on lateral and medial datasets separately. If these variables were not retained as explanatory variables in the regression model, analyses were run again pooling the lateral and medial datasets. The relative contribution of the variables were quantified by adjusted-R^2 (Adj-R^2) and root-mean-square-error ($RMSE$). To highlight the relative importance of the explanatory variables in the models, all the explanatory variables were normalized between -1 and 1. Data were considered statistically significant for $p < 0.05$. Statistical analyses were made using the Matlab 2017a Statistics Toolbox (Mathworks Inc., Natick, MA, USA).

2.8. Micromechanics modeling

The results of the statistical analysis presented in Sec. 3 suggest that the variability of all the stiffness constants can be explained by a small number of determinants, namely, the porosity (ϕ) and mineral content (DMB). This in turn suggests that the organization of the bone material follows a certain pattern, which we attempt to model following Grimal et al. [16]. We assume (1) that the vascular pore network can be modeled as a series of infinite cylindrical pores periodically distributed in bone matrix on a hexagonal lattice associated to porosity ϕ (Fig. 1 (h)); and (2) that the different elastic coefficients (stiffness tensor) of the bone matrix depend linearly on DMB (e.g., the amount of mineral scales the matrix elastic properties). The empirical relationships relating each elastic coefficient to DMB can be obtained straightforwardly taking $\phi = 0$ in equations 1- 5 (Table 5).

Specifically, the modeled effective stiffness constants C_{ij}^{cyl} are calculated using asymptotic homogenization [52, 53] (an implementation is available here [54]). The inputs of the model are ϕ, the stiffness of the material filling the pores (water of bulk modulus = 2.2 GPa and a null shear modulus), and the stiffness tensor of the matrix obtained as a function of DMB as explained above.

The quality of the model is evaluated by comparing C_{ij}^{cyl} to stiffness experimental data using linear regression and Bland-Altman plot.

3. Results

The specimens of one subject with a porosity higher than 30% was not included in the analysis. Two other subjects, for which part of the experiments failed due to damage to the specimens, were also excluded, which finally led to 26 subjects for each set (#1, #2 and #3) of specimens.

3.1. Descriptive statistics

The results of the elastic, microstructural and compositional (mineral and collagen) variables are summarized by the mean value and SD for the lateral and medial specimens, respectively, in Table 3. The microstructural variables (CV from 7.1% to 58.0%) and collagen (CV from 3.9% to 36.4%) showed a greater range of relative variability compared to the stiffness constants (CV from 6.4% to 14.2%) and mineral variables (CV from 1.4% to 5.6%). Significant differences were found between lateral and medial quadrants (Table 3) for two microstructure variables (ConnD, SMI) and the variables measured by FTIRM (MinOrga, MinMat, Carbon, CryInd and CollMat).

3.2. Univariate correlation analysis

Spearman rank correlation coefficients (R) between C_{ij} and the other variables are summarized in Table 4. For the variables displaying a significant difference between the lateral and medial quadrants, i.e., ConnD, SMI, MinOrga, MinMat, Carbon, CryInd and CollMat, R was calculated for lateral and medial group separately. Overall, the strongest correlations were found for the microstrucural variables and DMB. Among the microstructure variables, ϕ, PoN, and PoDm were negatively correlated with all the C_{ij} (R from -0.64 to -0.89). Positive correlations were found between PoS/PoV, PoSp, PoPf and all the C_{ij} (R from 0.50 to 0.86). ConnD from lateral quadrant significantly correlated with some C_{ij} (R from -0.41 to -0.55). Among the mineral variables, DMB was significantly correlated with all the C_{ij} (R from 0.77 to 0.81). MinOrga from lateral quadrant was significantly correlated with all the C_{ij} (R from 0.42 to 0.51). Moderate but significant correlation was found between

Table 3: A summary of the results (Mean(SD)) of stiffness constants, microstructure and compositional variables from the lateral (L) and medial (M) specimens. * Variables showing significant difference between lateral and medial specimen data and the corresponding p-values are also given below.

Stiffness constants

	C_{11} (GPa)	C_{33} (GPa)	C_{13} (GPa)	C_{44} (GPa)	C_{66} (GPa)
L	19.6(2.0)	29.0(2.3)	11.9(0.9)	5.8(0.6)	4.3(0.6)
M	20.1(1.8)	28.9(1.8)	12.1(0.9)	5.9(0.6)	4.5(0.6)

Microstructure variables

	ϕ (%)	PoS/PoV (mm^{-1})	PoN (mm^{-1})	PoDm (μm)	PoSp (μm)
L	7.4(4.3)	59.2(17.1)	0.78(0.25)	90(31)	323(35)
M	7.6(3.9)	61.8(19.7)	0.83(0.20)	89(34)	318(27)

	PoPf (mm^{-1})	ConnD* (mm^{-3}) $p < 1^{-7}$	SMI* (a.u.) $p = 0.01$	ρ (g/cm^3)
L	31.34(8.26)	10.3(5.0)	3.2(0.3)	1.90(0.06)
M	30.36(9.35)	24.8(5.8)	3.1(0.2)	1.90(0.06)

Mineral variables

	DMB (g/cm^3)	MinOrga* (n.u.) $p = 0.01$	MinMat* (n.u.) $p < 1^{-4}$	Carbon* (n.u.) $p < 1^{-6}$	CryInd* (cm) $p < 1^{-4}$
L	1.01(0.02)	5.26(0.30)	1.84(0.10)	0.0071(0.0003)	0.0384(0.0011)
M	1.02(0.02)	5.55(0.26)	1.72(0.07)	0.0066(0.0002)	0.0396(0.0006)

Collagen variables

	CollMat* (n.u.) $p = 0.005$	DHLNL (mmol/mol collagen)	HLNL (mmol/mol collagen)	PYD (mmol/mol collagen)	DPD (mmol/mol collagen)
L	4.54(0.37)	577.7(210.2)	265.1(78.6)	352.6(53.5)	98.3(17.5)
M	4.33(0.29)	557.9(183.5)	255.7(69.0)	353.5(34.3)	108.0(18.0)

	PEN (mmol/mol collagen)	Coll (%)
L	10.3(2.9)	13.6(0.8)
M	9.5(2.6)	13.4(0.5)

MinOrga and Carbon from medial quadrant and C_{13} ($R = 0.47$) and C_{44} ($R = -0.45$), respectively. Among the collagen variables, DHLNL and HLNL were significantly correlated with all the C_{ij} (R from -0.33 to -0.48), The variables that were not significantly correlated with any of the C_{ij}, i.e. SMI, MinMat, CryInd, CollMat, PYD, DPD, PEN and Coll were removed in the following regression analyses in Section 3.3. Additional information about the relationships between the variables within each group (C_{ij}, microstructure, mineral and

collagen) and among the groups can be found in Appendix B.

Table 4: Spearman correlation coefficient R between C_{ij} and microstructural, mineral and collagen variables. The variables with bold font were kept for the following analysis. Data from lateral and medial quadrants were analyzed separately for the variables who show significant differences between the two quadrants (additional labels 'L' and 'M' are added in the table). Results are not differentiated using labels 'L' and 'M' when no significant relationship was found both in the lateral and medial data. $^1p < 0.05$, $^2p < 0.001$, $^3p < 0.0001$, n.s. not significant.

		C_{11}	C_{33}	C_{13}	C_{44}	C_{66}
		-0.87^3	-0.80^3	-0.76^3	-0.89^3	-0.84^3
PoS/PoV		0.83^3	0.75^3	0.74^3	0.86^3	0.81^3
PoN		-0.74^3	-0.64^3	-0.66^3	-0.71^3	-0.69^3
PoDm		-0.77^3	-0.73^3	-0.67^3	-0.83^3	-0.77^3
PoSp		0.54^3	0.52^3	0.50^2	0.54^3	0.52^3
PoPf		0.81^3	0.72^3	0.72^3	0.82^3	0.78^3
ConnD	L	-0.41^1	-0.55^1	n.s.	-0.51^1	n.s.
	M	n.s.	n.s.	n.s.	n.s.	n.s.
SMI		n.s.	n.s.	n.s.	n.s.	n.s.
DMB		0.79^3	0.77^3	0.78^3	0.81^3	0.77^3
MinOrga	L	0.47^1	0.43^1	0.51^1	0.42^1	0.45^1
	M	n.s.	n.s.	0.47^1	n.s.	n.s.
MinMat		n.s.	n.s.	n.s.	n.s.	n.s.
Carbon	L	n.s.	n.s.	n.s.	n.s.	n.s.
	M	n.s.	n.s.	n.s.	-0.45^1	n.s.
CryInd		n.s.	n.s.	n.s.	n.s.	n.s.
CollMat		n.s.	n.s.	n.s.	n.s.	n.s.
DHLNL		-0.45^2	-0.44^2	-0.48^2	-0.44^1	-0.40^1
HLNL		-0.41^1	-0.41^1	-0.41^1	-0.40^1	-0.33^1
PYD		n.s.	n.s.	n.s.	n.s.	n.s.
DPD		n.s.	n.s.	n.s.	n.s.	n.s.
PEN		n.s.	n.s.	n.s.	n.s.	n.s.
Coll		n.s.	n.s.	n.s.	n.s.	n.s.

3.3. Multivariate regression model

In the multivariate regression models, bone stiffness constants C_{ij} are the dependent variables and the microstructure, mineral and collagen variables are the independent variables. None of the variables showing a significant difference between lateral and medial data and kept for multivariate regression analyses, i.e., ConnD, MinOrga and Carbon (Table 4), were retained after analyses. Therefore, the following results (Table 5) were obtained using the pooled data from lateral and medial quadrants.

Overall, ϕ and DMB were the most significant factors contributing to the variability of

the C_{ij}. In the multiple regression models using microstructure variables, ϕ explained most of the variability of the C_{ij} (Adj-R^2 from 58.8% to 84.4%), see Table 5. Among the mineral variables, DMB was the most significant factor explaining the variability of the C_{ij} (Adj-R^2 from 54.6% to 65.9%). As for the collagen variables, the only significant variable was DHLNL which only accounted for a minor part of the variability of the C_{ij} (Adj-R^2 from 9.9% to 21.8%). Aside from ϕ, DMB and DHLNL, PoPf in multiple regression model combining the microstructural variables was the only contributing variables to C_{33}. The regression coefficients of the variables in the linear model tell that the relative contribution of ϕ was greater than that of the other explanatory variables. In addition, PoPf and ϕ being strongly correlated ($R = 0.96$, see Appendix B), ϕ was the only microstructural variable used in the subsequent multiple linear regression analyses. Pooling together the explanatory variables from each group, ϕ, DMB and DHLNL, only two variables ϕ and DMB were retained as the best combination in the regression models which explained 76.1 to 90.9% of the variability of the C_{ij} (Table 5). The relative and combined contribution of ϕ and DMB to C_{ij} are illustrated in Figure 3.

3.4. Comparison between micromechanics model and experimental data

All the modeled stiffness constants C_{ij}^{cyl} were highly correlated to their experimental counterpart C_{ij} ($75.1\% < R^2 < 91.5\%$). The $RMSE$ ($0.18 < RMSE < 0.85$) and R^2 ($75.1\% < R^2 < 91.5\%$) between C_{ij}^{cyl} and C_{ij} present similar range as the results of the two-variable (ϕ and DMB) linear regression model ($0.18 < RMSE < 0.84$ and $76.4\% < R^2 < 90.9\%$) shown in Table 5. A bias of about 1.3 GPa was found between C_{11} and C_{11}^{cyl} and between C_{13} and C_{13}^{cyl} by the Bland-Altman's plots (not shown), whereas the bias on C_{33}^{cyl}, C_{44}^{cyl} and C_{66}^{cyl} ($d < 0.2$ GPa) are negligible.

4. Discussion

In this work, the relative contributions of the microstructure and composition to the mesoscale anisotropic elastic properties of human cortical bone in the elderly are investigated. To our knowledge, our study is the first one to provide data covering the complete anisotropic elastic tensor, the microstructure of cortical vascular porosity, mineral and collagen characteristics. One strength of the study is that all the physical quantities were obtained from the same specimens in each donor, or from immediately adjacent samples, which limits the confounding effect of material heterogeneity around the bone circumference and along the diaphysis. The anisotropic elastic properties have been measured by RUS, a technique newly introduced to measure bone elastic properties. The properties of the

Table 5: Multiple linear regression models of bone stiffness C_{ij}. In the two-variable models, only ϕ and DMB are included. Note that the explanatory variables with an overbar symbol have been normalized. [3] $p < 0.0001$.

Stiffness	Explanatory variables	Linear model	Adj-R^2 (%)	$RMSE$ (GPa)
C_{11}	microstructure	$18.14 - 4.06 \times \bar{\phi}$	78.9[3]	0.87
	mineral	$19.38 + 3.63 \times \overline{\text{DMB}}$	59.8[3]	1.20
	collagen	$19.48 - 1.34 \times \overline{\text{DHLNL}}$	13.0[1]	1.77
	ϕ + DMB	$18.36 - 3.03 \times \bar{\phi} + 1.66 \times \overline{\text{DMB}}$ (1)	86.4[3]	0.70
C_{33}	microstructure	$26.23 - 5.97 \times \bar{\phi} - 1.52 \times \overline{\text{PoPf}}$	82.0[3]	0.87
	mineral	$28.50 + 3.61 \times \overline{\text{DMB}}$	50.0[3]	1.45
	collagen	$28.57 - 1.47 \times$DHLNL	13.2[1]	1.91
	ϕ + DMB	$27.27 - 3.67 \times \bar{\phi} + 1.22 \times \overline{\text{DMB}}$ (2)	83.2[3]	0.84
C_{13}	microstructure	$11.31 - 1.67 \times \bar{\phi}$	58.8[3]	0.58
	mineral	$11.78 + 1.81 \times \overline{\text{DMB}}$	65.9[3]	0.53
	collagen	$11.79 - 0.80 \times \overline{\text{DHLNL}}$	21.8[1]	0.80
	ϕ + DMB	$11.47 - 0.92 \times \bar{\phi} + 1.21 \times \overline{\text{DMB}}$ (3)	76.4[3]	0.44
C_{44}	microstructure	$5.28 - 1.33 \times \bar{\phi}$	84.4[3]	0.24
	mineral	$5.69 + 1.16 \times \overline{\text{DMB}}$	60.6[3]	0.38
	collagen	$5.73 - 0.43 \times \overline{\text{DHLNL}}$	13.3[1]	0.56
	ϕ + DMB	$5.35 - 1.02 \times \bar{\phi} + 0.49 \times \overline{\text{DMB}}$ (4)	90.9[3]	0.18
C_{66}	microstructure	$3.86 - 1.29 \times \bar{\phi}$	76.1[3]	0.30
	mineral	$4.25 + 1.16 \times \overline{\text{DMB}}$	58.8[3]	0.39
	collagen	$4.30 - 0.39 \times \overline{\text{DHLNL}}$	9.9[1]	0.58
	ϕ + DMB	$3.93 - 0.95 \times \bar{\phi} + 0.55 \times \overline{\text{DMB}}$ (5)	83.7[3]	0.25

vascular pore network and mineral content have been assessed using SR-μCT, a reference method for these purposes [55].

The data was obtained on cadaveric bones from elderly donors without documentation on the existence of bone pathologies. It follows that the dataset of this study provides reference nominal values and ranges of variations for this population, which information is critical to interpret data from donors with pathologies.

Recently, RUS was successfully developed to characterize the anisotropic stiffness of human cortical bone [35, 38] and to investigate the elasticity-density relationship of human tibial cortical bone specimens [56]. Based on its good accuracy and ease of use, RUS is emerging as the technique of choice for investigating the stiffness of small-sized bone specimens. Because the full set of the elastic tensor can be identified using RUS, the engineering moduli which are often used in evaluating bone mechanical properties such as stress and strain, can also be derived.

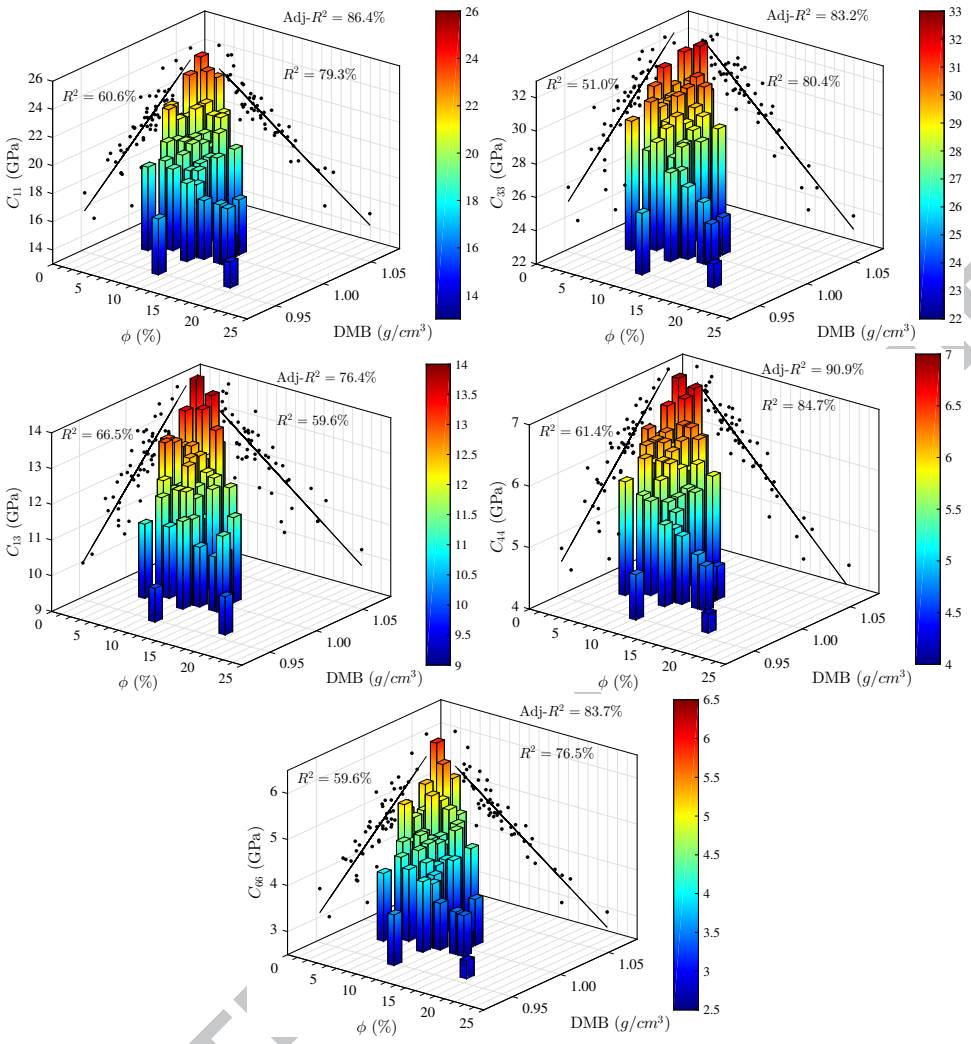

Figure 3: 3D bar graphs representing the C_{ij} as a function of ϕ and DMB. Linear regressions are plotted in the background for each variable with the coefficients of determination (R^2) and the Adj-R^2 values of the model using ϕ and DMB as the explanatory variables are depicted as well.

The experimental errors using RUS are well documented [40, 57] and are typically low (approximately 1.7% for the shear stiffness constants and approximately 3.1% for the longitudinal and off-diagonal stiffness constants) compared to other techniques available for 'small' specimens (a few mm^3). Furthermore, the measurement is quick (a few minutes per specimen) so that the technique can be used routinely.

Comparing the data from lateral and medial quadrants, no significant difference was observed in stiffness, DMB, collagen variables and most of the microstructural variables. Though a significant difference was observed for the mineral variables measured by FTIRM between the two sites, this difference was not found in DMB and was not appreciated by the stiffness as there was no significant difference for stiffness either.

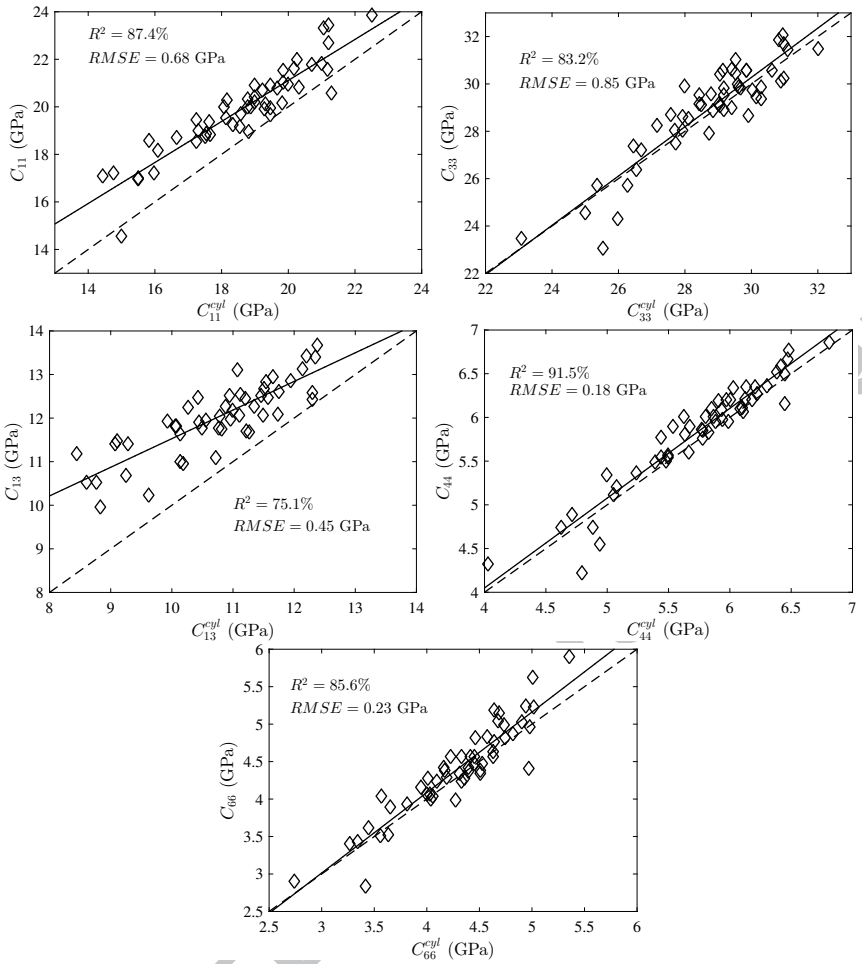

Figure 4: Linear regression between the C_{ij} and C^{cyl}_{ij}. Solid line is the regression model and dash line is $y = x$ line.

Linear relationships were assumed between bone properties in the statistical analyses. Previous work showed that power functions may be more appropriate to account for micromechanics relations between porosity and elasticity for porous material in a wide range of porosity values (0-100%) [58]. However, the range of cortical porosity values is limited in this work (less than 22%) and a linear relationship can be considered in this limited region for statistical analyses, as observed in our data as well as in others' [21]. Linear correlations chosen for this work provide models with R^2 (for the best model) typically higher than 0.8 and $RMSE$ between 0.18 and 0.84 GPa which indicates that the linear models are appropriate.

Among the variables in the mineral group, significant correlations with C_{ij} were observed only for DMB, MinOrga and Carbon. We found that DMB exhibits a limited range of variations between individuals in the adults, which is consistent with literature data [27, 59]. Despite this small range of variation, we could observe, for the first time, that the volumetric

DMB measured by SR-μCT on human femur correlates with all the mesoscopic stiffness constants. This is consistent with the studies directly relating bone elastic properties with ash density [25, 26]. Although previous studies showed that MinOrga, CollMat and CyrstInd measured by FTIRM may explain part of the variability of the micromechanical properties of bone tissue [32, 60], such an effect was not observed for bone mesoscopic elastic properties in our data. The influence of porosity is so predominant in determining mesoscopic stiffness of our sample set that a correlation between other variables and mesoscopic stiffness can be difficult to observe, especially if they are not measured exactly in the same place, as it is the case for stiffness and mineral properties.

For the collagen variables, we did not find correlation between mature enzymatic cross-links PYD, DPD, non-enzymatic PEN, collagen amount (Coll) and any of the C_{ij} which is consistent with previous observations [27, 61]. However, we observed significant correlations between immature enzymatic cross-links DHLNL, HLNL and all the C_{ij} (R between -0.33 and -0.48, Table 4) which has not been observed before. One may also observe that, while both DHLNL and HLNL are correlated with the C_{ij}, none of these variables was retained in the best multiple regression model. DHLNL and HLNL are highly correlated together ($R = 0.94$, Table B.7) and with DMB ($R = 0.55$, Table B.7), hence they may be replaced by the more predominant explanatory variable DMB. Indeed, after the adjustment for DMB, DHLNL and HLNL do not correlated with any of the C_{ij}. Another interesting observation is that we found a significant correlation between ϕ and DMB ($R = -0.59$, Table B.6) which was not observed before.

The microstructure variables explain a major part of the variability of C_{ij} (Table 4). Note that the variability in microstructure are more important than the variability in mineral properties in the elderly. Regarding this point, to the best of our knowledge, the only study that compares to ours is that of Bala et al. [24] investigating the influence of the pore network architecture on the human cortical bone elasticity measured at the fibula. Overall, our results are consistent with those reported in Bala's study, despite some differences in the absolute value of the measured variables and correlations, which can be explained by differences in skeletal site and measurement methods.

An important finding of the study is that, among all the variables investigated which reflect the microstructure and chemical composition of bone, only two (ϕ and DMB) independently contribute to the variability of the stiffness constants (Table 5). ϕ and DMB alone explain $59.6 - 84.7\%$ and $51.0 - 66.5\%$ of the variability of C_{ij}, respectively (Fig. 3).

Once the most important determinants of bone stiffness are determined, one should be able to design a simplified model based on these determinants to predict bone stiffness. One approach for heterogeneous media like bone is through homogenization. Several ho-

mogenization scheme exists, such as Mori-Tanaka [62], asymptotic homogenization [52, 53] and fast fourier transform based homogenization [63]. In this work we modeled the vasular pore network as a series of infinite cylindrical pores periodically distributed in bone matrix and chose an asymptotic homogenization method. Although bone microstructure as that shown in Figure 1(a) is not strictly a periodic arrangement of Haversian canals, it has been shown that the asymptotic homogenization and a random homogenization approach such as Mori-Tanaka homogenization yield almost identical results for cortical bone [53]. In the model, bone matrix elasticity should be known beforehand to calculate the effective stiffness constants C_{ij}^{cyl}. Considering that the C_{ij} are well predicted by a multilinear models with ϕ and DMB as explanatory variables, estimates of the matrix stiffness constants C_{ij}^{m} can be obtained by extrapolation to null porosity of equations 1- 5.

Modeling the vascular porosity as a network of cylindrical pores is a commonly used model, e.g., by Grimal et al. [16], Fritsch and Hellmich [64], Deuerling et al. [65]. Granke et al. [22] found that this model can be used to reproduce the variation of elastic coefficients with porosity assuming fixed values of the matrix elastic coefficients for a collection of specimens. Deuerling et al. [65] used a similar model to account for the combined variations of porosity and average orientation of the mineral crystals. In the present study, for the first time as far as we know, the elastic properties of matrix were scaled on the mineral content. This approach is consistent with several studies showing that the matrix elasticity probed with nanoindentation [66] or acoustic microscopy [67] is correlated to the mineral content. The predicted C_{ij}^{cyl} were found to be in good agreement with the measured values C_{ij} demonstrating the ability of the two-parameter micromechanical model to account for the variations of bone anisotropic stiffness. Nevertheless, one needs to notice that one important microstructure feature of cortical bone, Volkman's canals which are oriented roughly perpendicular to the osteons, is not accounted for in the cylindrical model. This may explain some difference observed between C_{ij}^{cyl} and C_{ij}. This point was also discussed in [68].

With the complete set of the anisotropic elastic tensor, engineering moduli (Young's moduli and Poisson's ratios) can be converted. Following the same statistical analyses strategy, cortical porosity and DMB were found as the most important determinants of engineering moduli as well. As all the data used in the manuscript including the engineering moduli are provided in the supplementary material. The analysis for engineering moduli is not detailed in the manuscript.

Several limitations in this work should be pointed out. Investigating the relationships between several bone characteristics would ideally require that these characteristics are measured on the same specimens. For technical reasons, not all variables could be measured

exactly in the same location. The C_{ij} , microstructural variables and DMB were measured on the same specimens (set #1), whereas the other mineral and collagen variables were measured on different set of specimens (set #2 and #3). For example, the distance between the samples #1 for the measurement of stiffness and microstructure and the samples #3 for the measurement of the mineral was of the order of 25 mm. In the mid-diaphysis of human femoral bone, such a distance between two measurement points can induce about 8% differences in cortical bone elasticity [37, 69]. The homogeneity of other bone characteristics along the axis is however unknown. Such inhomogeneity of bone properties along the axis is expected to weaken the observable correlations between variables measured at different locations. Note that the variables selected in the optimal multiple regression models (porosity, DMB) and the stiffness constants were all measured on the same set of specimens (#1).

Bone mesoscopic stiffness is potentially influenced by other compositional and organizational features than those reported here. These include microporosity [70], size of the mineral crystals [71], collagen fibrils orientation [72, 73] and other matrix constituents such as water content which has been reported to affect microscopic stiffness [74]. Microporosity, is constituted by osteocytes lacunae and canaliculi, whose size is small to an extent that is below the spatial resolution of SR-μCT and hence it precludes an accurate quantification with this imaging modality. However, because microporosity accounts for a minor part of total cortical porosity, i.e., less than 1% for lacunar porosity [75], and about 1% for canaliculi porosity [76], we hypothesized that its influence on stiffness could be neglected in first approximation. The size of the mineral crystals and collagen fibril orientation were not available at the time of this study. Our results showing that a combination of ϕ and DMB explains most of the variance of the stiffness coefficient (Adj-R^2 from 76% to 91%) suggests that the contribution of these latter two variables to stiffness is likely to be of weak importance, at least in the samples studied here.

The bone specimens were collected on a single skeletal site and the pathological status of the donors is unknown. Other studies have shown that bone diseases or drug treatment could alter the compositional properties [32, 33] and herein may lead to different results. In children's cortical bone, different bone characteristics were observed compared to adults' cortical bone [24, 77]. Therefore, the findings in this work should be limited to the femoral mid-diaphysis of an aged group of donors. In addition, in this study, we did not analyze the influence of age, sexual dimorphism of male/female bone and post-menopausal bone loss in females because this study was not designed for these purposes.

Another limitation is that the effect of the orientation of the mineralized collagen fiber was not investigated. Previous studies have shown that the elastic modulations of bone

lamellae are mainly determined by the fibril arrangement [72, 73] rather than compositional variations. It may be worth investigating if the variations in fibril arrangement exist also among individuals and if this variations incorporating bone microstructure would affect bone elasticity at the mesoscale.

It is worthwhile to mention some perspectives given that a comprehensive list of bone properties has been measured: (i) as the stiffness properties measured by RUS are related to both the microscale elastic properties and the pore network, a perspective is to infer thesample specific matrix properties from the RUS data and porous network images [78]; (ii) as the post-yield and failure properties were also assessed by toughness experiments [48] on specimen #2, relationships between elastic properties obtained in the current study toughness properties, and compression strength will be analyzed in a further work; (iii) regarding prediction models of failure properties for clinical applications incorporating the data provided in this work, difficulties still remain in the *in vivo* assessment of many bone properties, such as collagen or mineral properties.

5. Conclusion

This study reveals that cortical vascular porosity and DMB are the most important determinants of cortical bone anisotropic mesoscopic stiffness and that the relative contribution of porosity is higher than that of DMB. This conclusion may apply only to the population studied in this work. Detailed knowledge of bone microstructure features, such as pore number and pore diameter may not be necessary to predict mesoscopic bone stiffness in the elderly. The presented data can help to form a better understanding of the relationships between bone stiffness on one hand and microstructure and composition on the other hand and help to develop biomechanical models for bone. Also, this work presents reference values for the range of variation of a number of bone characteristics at the femoral mid-diaphysis in the elderly.

Acknowledgment

The authors thank the ESRF for allocated beam time within the experiments MD 927 on beam line ID 19 and MD 1056 on beam line ID 17. We also acknowledge the support of Lukas Helfen on beam line ID 19, as well as Herwig Requardt and Alberto Bravin on beam line ID 17. This work received financial support from the French National Research Agency (ANR) under the MULTIPS project (ANR-13-BS09-0006) and was performed within the framework of the LABEX PRIMES (ANR-11-LABX-0063) of the Université de Lyon, within the program "Investissements d'Avenir" (ANR-11-IDEX-0007).

Appendix A. Additional information on RUS

For a solid free vibrating elastic body with given elasticity and rectangular parallelepiped geometry, the resonant frequencies f^{cal} can be calculated by solving the equations of motion using Rayleigh-Ritz method [79]. The stiffness constants can be determined by minimizing the distance between measured resonant frequencies f^{exp} and calculated resonant frequencies (inverse problem):

$$F(C_{ij}) = \sum_{k=1}^{n} \left(\frac{f_k^{exp} - f_k^{cal}(C_{ij})}{f_k^{exp}} \right)^2 \tag{A.1}$$

where k is the index of the resonant frequencies and n is the number of resonant frequencies used in the inverse problem. RUS experiments were performed and the inverse problem was solved following [35, 38, 80] as detailed in Section 2.2. For orthotropic elastic symmetry or higher symmetry, the engineering moduli such as Young's moduli and Poisson's ratios which are more often evaluated in a mechanical testing experiment can be converted knowing all the stiffness constants [5].

Appendix B. Correlations between the bone characteristics

The focus of this work was placed on the relationships between bone stiffness and microstruactural, compositional properties. We also observed interesting correlations within and among each group of the variables. Spearman correlation coefficients between the variables in each group as well as between the groups are listed bellow, from Tables B.6 to B.9. Note that for the variables whose data from lateral site are significantly different from the data from medial site, the correlations were calculated using the datasets from lateral or medial only.

Table B.6: Spearman correlation coefficient R between microstructure variables and between microstructure, mineral and collagen variables. $^{1}p < 0.05$, $^{2}p < 0.001$, $^{3}p < 0.0001$, n.s. not significant.

	ϕ	PoS/PoV	PoN	PoDm	PoSp	PoPf	ConnD	SMI
PoS/PoV	-0.95^{3}	-	-	-	-	-	-	-
PoN	0.80^{3}	-0.67^{3}	-	-	-	-	-	-
PoDm	0.90^{3}	-0.95^{3}	0.50^{2}	-	-	-	-	-
PoSp	-0.47^{2}	n.s.	-0.60^{3}	-0.28^{1}	-	-	-	-
PoPf	-0.96^{3}	0.95^{3}	-0.81^{3}	-0.85^{3}	0.29^{1}	-	-	-
ConnD L	0.51^{1}	-0.40^{1}	0.65^{1}	n.s.	-0.63^{1}	-0.48^{1}	-	-
ConnD M	n.s.	n.s.	n.s.	n.s.	-0.51^{1}	-0.48^{1}	-	-
SMI L	n.s.	n.s.	-0.44^{1}	n.s.	n.s.	n.s.	n.s.	-
SMI M	n.s.	n.s.	-0.45^{1}	n.s.	n.s.	n.s.	n.s.	-
DMB	-0.59^{3}	0.55^{3}	-0.51^{3}	-0.53^{3}	0.54^{3}	0.53^{3}	n.s.	n.s.
MinOrga L	n.s.	n.s.	-0.53^{1}	n.s.	0.57^{1}	n.s.	n.s.	n.s.
MinOrga M	n.s.	n.s.	n.s.	n.s.	n.s.	n.s.	n.s.	n.s.
MinMat L	n.s.	n.s.	n.s.	n.s.	n.s.	n.s.	-0.48^{1}	n.s.
MinMat M	n.s.	n.s.	n.s.	n.s	0.40^{1}	n.s.	-0.40^{1}	n.s.
Carbon L	n.s.	n.s.	n.s.	n.s.	n.s.	n.s.	n.s.	n.s.
Carbon M	n.s.	n.s.	n.s.	n.s.	-0.49^{1}	n.s.	n.s.	n.s.
CryInd L	n.s.	n.s.	n.s.	n.s.	n.s.	n.s.	n.s.	n.s.
CryInd M	n.s.	n.s.	n.s.	n.s.	n.s.	n.s.	n.s.	n.s.
CollMat L	n.s.	n.s.	n.s.	n.s.	n.s.	n.s.	n.s.	n.s.
CollMat M	n.s.	n.s.	n.s.	n.s.	n.s.	n.s.	n.s.	n.s.
DHLNL	n.s.	n.s.	0.44^{1}	n.s.	-0.57^{3}	n.s.	n.s.	n.s.
HLNL	n.s.	n.s.	0.44^{1}	n.s.	-0.46^{2}	n.s.	n.s.	n.s.
PYD	n.s.	n.s.	n.s.	n.s.	-0.32^{1}	n.s.	n.s.	n.s.
DPD	n.s.	n.s.	n.s.	n.s.	n.s.	n.s.	n.s.	-0.34^{1}
PEN	n.s.	n.s.	-0.27^{1}	n.s.	n.s.	n.s.	n.s.	n.s.
Coll	-0.28^{1}	n.s.	n.s.	n.s.	n.s.	0.28^{1}	n.s.	n.s.

Table B.7: Spearman correlation coefficient R between collagen variables. $^1p < 0.05$, $^2p < 0.001$, $^3p < 0.0001$, n.s. not significant.

	DHLNL	HLNL	PYD	DPD	PEN	Coll
HLNL	0.94^3	-	-	-	-	-
PYD	0.53^3	0.37^1	-	-	-	-
DPD	n.s.	n.s.	0.54^3	-	-	-
PEN	-0.52^3	-0.56^3	n.s.	n.s.	-	-
Coll	n.s.	n.s.	n.s.	n.s.	n.s.	-
DMB	-0.55^3	-0.56^3	n.s.	n.s.	0.34^1	n.s.
MinOrga L	-0.52^1	-0.48^1	n.s.	n.s.	0.40^1	n.s.
MinOrga M	-0.54^1	-0.55^1	n.s.	n.s.	0.60^1	n.s.
MinMat L	n.s.	n.s.	n.s.	n.s.	n.s.	n.s.
MinMat M	n.s.	n.s.	n.s.	n.s.	n.s.	0.39^1
Carbon L	n.s.	n.s.	n.s.	n.s.	n.s.	n.s.
Carbon M	n.s.	n.s.	n.s.	n.s.	n.s.	n.s.
CryInd L	n.s.	n.s.	n.s.	n.s.	n.s.	n.s.
CryInd M	n.s.	n.s.	n.s.	n.s.	n.s.	n.s.
CollMat L	n.s.	n.s.	n.s.	n.s.	n.s.	n.s.
CollMat M	n.s.	n.s.	n.s.	n.s.	n.s.	n.s.

Table B.8: Spearman correlation coefficient R between mineral variables and between mineral and collagen variables. $^1p < 0.05$, $^2p < 0.001$, $^3p < 0.0001$, n.s. not significant.

	DMB	MinOrgan	MinMat	Carbon	CryInd	CollMat
MinOrga L	0.51^1	-	-	-	-	-
MinOrga M	0.66^2	-	-	-	-	-
MinMat L	n.s.	n.s.	-	-	-	-
MinMat M	n.s.	n.s.	-	-	-	-
Carbon L	n.s.	-0.44^1	n.s.	-	-	-
Carbon M	n.s.	n.s.	n.s.	-	-	-
CryInd L	n.s.	n.s.	0.62^2	-0.59^1	-	-
CryInd M	n.s.	n.s.	n.s.	-0.53^1	-	-
CollMat L	n.s.	n.s.	0.42^1	n.s.	n.s.	-
CollMat M	n.s.	n.s.	n.s.	n.s.	n.s.	-

Table B.9: Spearman correlation coefficient R between C_{ij}. $^3p < 0.0001$.

	C_{11}	C_{33}	C_{13}	C_{44}	C_{66}
C_{33}	0.79^3	-	-	-	-
C_{13}	0.91^3	0.76^3	-	-	-
C_{44}	0.94^3	0.90^3	0.87^3	-	-
C_{66}	0.97^3	0.74^3	0.89^3	0.93^3	-

References

[1] P. Augat, S. Schorlemmer, The role of cortical bone and its microstructure in bone strength, Age and ageing 35 (2006) ii27–ii31.

[2] J. D. Currey, Biomechanics of mineralized skeletons, Wiley Online Library, New York, 1990, pp. 11–25.

[3] P. Fratzl, R. Weinkamer, Nature's hierarchical materials, Progress in Materials Science 52 (2007) 1263–1334.

[4] M.-M. Giraud-Guille, Twisted plywood architecture of collagen fibrils in human compact bone osteons, Calcified tissue international 42 (1988) 167–180.

[5] S. C. Cowin, Bone mechanics handbook, CRC press, 2001.

[6] J. Y. Rho, L. Kuhn-Spearing, P. Zioupos, Mechanical properties and the hierarchical structure of bone, Medical engineering and physics 20 (1998) 92–102.

[7] R. Chapurlat, In vivo evaluation of bone microstructure in humans: Clinically useful?, BoneKEy reports 5 (2016) 813.

[8] G. Holzer, G. von Skrbensky, L. A. Holzer, W. Pichl, Hip fractures and the contribution of cortical versus trabecular bone to femoral neck strength, Journal of bone and mineral research 24 (2009) 468–474.

[9] S. D. Rockoff, E. Sweet, J. Bleustein, The relative contribution of trabecular and cortical bone to the strength of human lumbar vertebrae., Calcified tissue research 3 (1969) 163–175.

[10] L. Vico, M. Zouch, A. Amirouche, D. Frère, N. Laroche, B. Koller, A. Laib, T. Thomas, C. Alexandre, High-resolution pqct analysis at the distal radius and tibia discriminates patients with recent wrist and femoral neck fractures., Journal of bone and mineral research 23 (2008) 1741–1750.

[11] Y. Bala, R. Zebaze, A. Ghasem-Zadeh, E. J. Atkinson, S. Iuliano, J. M. Peterson, S. Amin, s. Bjørnerem, L. J. Melton, H. Johansson, J. A. Kanis, S. Khosla, E. Seeman, Cortical porosity identifies women with osteopenia at increased risk for forearm fractures., Journal of bone and mineral research 29 (2014) 1356–1362.

[12] E. Sornay-Rendu, J.-L. Cabrera-Bravo, S. Boutroy, F. Munoz, P. D. Delmas, Severity of vertebral fractures is associated with alterations of cortical architecture in postmenopausal women., Journal of bone and mineral research 24 (2009) 737–743.

[13] P. Szulc, S. Boutroy, N. Vilayphiou, A. Chaitou, P. D. Delmas, R. Chapurlat, Cross-sectional analysis of the association between fragility fractures and bone microarchitecture in older men: the strambo study., Journal of bone and mineral research 26 (2011) 1358–1367.

[14] E. Sornay-Rendu, S. Boutroy, F. Duboeuf, R. D. Chapurlat, Bone microarchitecture assessed by hr-pqct as predictor of fracture risk in postmenopausal women: The ofely study., Journal of bone and mineral research 32 (2017) 1243–1251.

[15] E. J. Samelson, K. E. Broe, H. Xu, L. Yang, S. Boyd, E. Biver, P. Szulc, J. Adachi, S. Amin, E. Atkinson, C. Berger, L. Burt, R. Chapurlat, T. Chevalley, S. Ferrari, D. Goltzman, D. A. Hanley, M. T. Hannan, S. Khosla, C.-T. Liu, M. Lorentzon, D. Mellstrom, B. Merle, M. Nethander, R. Rizzoli, E. Sornay-Rendu, B. Van Rietbergen, D. Sundh, A. K. O. Wong, C. Ohlsson, S. Demissie, D. P. Kiel, M. L. Bouxsein, Cortical and trabecular bone microarchitecture as an independent predictor of incident fracture risk in older women and men in the bone microarchitecture international consortium (bomic): a prospective study., The lancet. Diabetes & endocrinology 7 (2019) 34–43.

[16] Q. Grimal, G. Rus, W. J. Parnell, P. Laugier, A two-parameter model of the effective elastic tensor for cortical bone, Journal of biomechanics 44 (2011) 1621–1625.

[17] J. D. Currey, Bones: structure and mechanics, Princeton university press, Princeton, 2002.

[18] D. Rohrbach, Q. Grimal, P. Varga, F. Peyrin, M. Langer, P. Laugier, K. Raum, Distribution of mesoscale elastic properties and mass density in the human femoral shaft, Connective tissue research 56 (2015) 120–132.

[19] J. D. Currey, The effects of strain rate, reconstruction and mineral content on some mechanical properties of bovine bone, Journal of biomechanics 8 (1975) 8183–8286.

[20] D. R. Carter, W. C. Hayes, The compressive behavior of bone as a two-phase porous structure., Journal of Bone and Joint Surgery 59 (1977) 954–962.

[21] X. N. Dong, X. E. Guo, The dependence of transversely isotropic elasticity of human femoral cortical bone on porosity, Journal of biomechanics 37 (2004) 1281–1287.

[22] M. Granke, Q. Grimal, A. Saïed, P. Nauleau, F. Peyrin, P. Laugier, Change in porosity is the major determinant of the variation of cortical bone elasticity at the millimeter scale in aged women, Bone 49 (2011) 1020–1026.

[23] D. M. Cooper, C. D. L. Thomas, J. G. Clement, A. L. Turinsky, C. W. Sensen, B. Hallgrímsson, Age-dependent change in the 3d structure of cortical porosity at the human femoral midshaft, Bone 40 (2007) 957–965.

[24] Y. Bala, E. Lefèvre, J.-P. Roux, C. Baron, P. Lasaygues, M. Pithioux, V. Kaftandjian, H. Follet, Pore network microarchitecture influences human cortical bone elasticity during growth and aging, Journal of the mechanical behavior of biomedical materials 63 (2016) 164–173.

[25] J. D. Currey, The effect of porosity and mineral content on the young's modulus of elasticity of compact bone, Journal of biomechanics 21 (1988) 131 – 139.

[26] C. Öhman, M. Baleani, C. Pani, F. Taddei, M. Alberghini, M. Viceconti, M. Manfrini, Compressive behaviour of child and adult cortical bone, Bone 49 (2011) 769–776.

[27] H. Follet, S. Viguet-Carrin, B. Burt-Pichat, B. Dépalle, Y. Bala, E. Gineyts, F. Munoz, M. Arlot, G. Boivin, R. D. Chapurlat, P. D. Delmas, M. L. Bouxsein, Effects of preexisting microdamage, collagen cross-links, degree of mineralization, age, and architecture on compressive mechanical properties of elderly human vertebral trabecular bone., Journal of orthopaedic research 29 (2011) 481–488.

[28] S. Nuzzo, F. Peyrin, P. Cloetens, J. Baruchel, G. Boivin, Quantification of the degree of mineralization of bone in three dimensions using synchrotron radiation microtomography, Medical physics 29 (2002) 2672–2681.

[29] X. Banse, T. Sims, A. Bailey, Mechanical properties of adult vertebral cancellous bone: correlation with collagen intermolecular cross-links, Journal of Bone and Mineral Research 17 (2002) 1621–1628.

[30] H. Oxlund, M. Barckman, G. Ørtoft, T. Andreassen, Reduced concentrations of collagen cross-links are associated with reduced strength of bone, Bone 17 (1995) S365–S371.

[31] M. Vanleene, A. Porter, P.-V. Guillot, A. Boyde, M. Oyen, S. Shefelbine, Ultrastructural defects cause low bone matrix stiffness despite high mineralization in osteogenesis imperfecta mice, Bone 50 (2012) 1317–1323.

[32] Y. Bala, B. Depalle, D. Farlay, T. Douillard, S. Meille, H. Follet, R. Chapurlat, J. Chevalier, G. Boivin, Bone micromechanical properties are compromised during long-term alendronate therapy independently of mineralization, Journal of Bone and Mineral Research 27 (2012) 825–834.

[33] S. Ma, E. L. Goh, A. Jin, R. Bhattacharya, O. R. Boughton, B. Patel, A. Karunaratne, N. T. Vo, R. Atwood, J. P. Cobb, U. Hansen, R. L. Abel, Long-term effects of bisphosphonate therapy: perforations, microcracks and mechanical properties., Scientific reports 7 (2017) 43399.

[34] R. Gauthier, H. Follet, M. Langer, S. Meille, J. Chevalier, F. Rongiéras, F. Peyrin, D. Mitton, Strain rate influence on human cortical bone toughness: A comparative study of four paired anatomical sites, Journal of the mechanical behavior of biomedical materials 71 (2017) 223–230.

[35] S. Bernard, Q. Grimal, P. Laugier, Accurate measurement of cortical bone elasticity tensor with resonant ultrasound spectroscopy, Journal of the mechanical behavior of biomedical materials 18 (2013) 12–19.

[36] H. S. Yoon, J. L. Katz, Ultrasonic wave propagation in human cortical bone - ii. measurements of elastic properties and microhardness, Journal of biomechanics 9 (1976) 459–464.

[37] A. A. E. Orías, J. M. Deuerling, M. D. Landrigan, J. E. Renaud, R. K. Roeder, Anatomic variation in the elastic anisotropy of cortical bone tissue in the human femur, Journal of the mechanical behavior of biomedical materials 2 (2009) 255–263.

[38] S. Bernard, G. Marrelec, P. Laugier, Q. Grimal, Bayesian normal modes identification and estimation of elastic coefficients in resonant ultrasound spectroscopy, Inverse Problems 31 (2015) 065010.

[39] B. A. Auld, Acoustic fields and waves in solids, 2nd edition, volume 1, Krieger, Malabar, Florida, 1990.

[40] X. Cai, L. Peralta, P.-J. Gouttenoire, C. Olivier, F. Peyrin, P. Laugier, Q. Grimal, Quantification of stiffness measurement errors in resonant ultrasound spectroscopy of human cortical bone, The Journal of the Acoustical Society of America 142 (2017) 2755–2765.

[41] X. Cai, L. Peralta, A. Giron, L. Helfen, C. Olivier, F. Peyrin, P. Laugier, Q. Grimal, Cortical bone elasticity measured by resonant ultrasound spectroscopy is not altered by defatting and synchrotron x-ray imaging, Journal of the mechanical behavior of biomedical materials 72 (2017) 241–245.

[42] M. Salomé, F. Peyrin, P. Cloetens, C. Odet, A. M. Laval-Jeantet, J. Baruchel, P. Spanne, A synchrotron radiation microtomography system for the analysis of trabecular bone samples, Medical Physics 26 (1999) 2194–2204.

[43] T. Weitkamp, P. Tafforeau, E. Boller, P. Cloetens, J.-P. Valade, P. Bernard, F. Peyrin, W. Ludwig, L. Helfen, J. Baruchel, Status and evolution of the esrf beamline id19, in: X-ray Optics and Microanalysis: Proceedings of the 20th International Congress, volume 1221, 2010, pp. 33–38.

[44] A. Mirone, E. Brun, E. Gouillart, P. Tafforeau, J. Kieffer, The pyhst2 hybrid distributed code for high speed tomographic reconstruction with iterative reconstruction and a priori knowledge capabilities, Nuclear Instruments and Methods in Physics Research Section B: Beam Interactions with Materials and Atoms 324 (2014) 41–48.

[45] S. Nuzzo, M. Lafage-Proust, E. Martin-Badosa, G. Boivin, T. Thomas, C. Alexandre, F. Peyrin, Synchrotron radiation microtomography allows the analysis of three-dimensional microarchitecture and degree of mineralization of human iliac crest biopsy specimens: Effects of etidronate treatment, Journal of Bone and Mineral Research 17 (2002) 1372–1382.

[46] R. Blanchard, A. Dejaco, E. Bongaers, C. Hellmich, Intravoxel bone micromechanics for microct-based finite element simulations, Journal of biomechanics 46 (2013) 2710–2721.

[47] R. Blanchard, C. Morin, A. Malandrino, A. Vella, Z. Sant, C. Hellmich, Patient-specific fracture risk assessment of vertebrae: A multiscale approach coupling x-ray physics and continuum micromechanics., International journal for numerical methods in biomedical engineering 32 (2016).

[48] R. Gauthier, H. Follet, M. Langer, E. Gineyts, F. Rongiéras, F. Peyrin, D. Mitton, Relationships between human cortical bone toughness and collagen cross-links on paired anatomical locations, Bone 112 (2018) 202–211.

[49] S. Viguet-Carrin, E. Gineyts, C. Bertholon, P. Delmas, Simple and sensitive method for quantification of fluorescent enzymatic mature and senescent crosslinks of collagen in bone hydrolysate using single-column high performance liquid chromatography, Journal of Chromatography B 877 (2009) 1–7.

[50] E. Gineyts, O. Borel, R. Chapurlat, P. Garnero, Quantification of immature and mature collagen crosslinks by liquid chromatography–electrospray ionization mass spectrometry in connective tissues, Journal of Chromatography B 878 (2010) 1449–1454.

[51] M. Gardegaront, D. Farlay, O. Peyruchaud, H. Follet, Automation of the peak fitting method in bone ftir microspectroscopy spectrum analysis: Human and mice bone study, Journal of Spectroscopy 2018 (2018).

[52] W. J. Parnell, Q. Grimal, The influence of mesoscale porosity on cortical bone anisotropy. investigations via asymptotic homogenization, Journal of the Royal Society Interface 6 (2009) 97–109.

[53] W. J. Parnell, M. Vu, Q. Grimal, S. Naili, Analytical methods to determine the effective mesoscopic and macroscopic elastic properties of cortical bone, Biomechanics and modeling in mechanobiology 11 (2012) 883–901.

[54] Bonhomv1.3, https://lib.upmc.fr/~qgrimal/downloads.html (????).

[55] A. Ostertag, F. Peyrin, P. Gouttenoire, J. Laredo, M. DeVernejoul, M. C. Solal, C. Chappard, Multiscale and multimodality computed tomography for cortical bone analysis, Physics in Medicine and Biology 61 (2016) 8553.

[56] S. Bernard, J. Schneider, P. Varga, P. Laugier, K. Raum, Q. Grimal, Elasticity-density and viscoelasticity-density relationships at the tibia mid-diaphysis assessed from resonant ultrasound spectroscopy measurements., Biomechanics and Modeling in Mechanobiology 15 (2016) 97–109.

[57] A. Migliori, J. D. Maynard, Implementation of a modern resonant ultrasound spectroscopy system for the measurement of the elastic moduli of small solid specimens, Review of Scientific Instruments 76 (2005) 121301.

[58] A. Fritsch, C. Hellmich, P. Young, Micromechanics-derived scaling relations for poroelasticity and strength of brittle porous polycrystals, Journal of Applied Mechanics 80 (2013) 020905.

[59] R. W. McCalden, J. A. McGeough, M. B. Barker, C. M. Court-Brown, Age-related changes in the tensile properties of cortical bone. the relative importance of changes in porosity, mineralization, and microstructure., The Journal of bone and joint surgery. American volume 75 (1993) 1193–1205.

[60] Y. Bala, D. Farlay, G. Boivin, Bone mineralization: from tissue to crystal in normal and pathological contexts, Osteoporosis International 24 (2013) 2153–2166.

[61] D. Vashishth, G. Gibson, J. Khoury, M. Schaffler, J. Kimura, D. Fyhrie, Influence of nonenzymatic glycation on biomechanical properties of cortical bone, Bone 28 (2001) 195–201.

[62] T. Mori, K. Tanaka, Average stress in matrix and average elastic energy of materials with misfitting inclusions, Acta metallurgica 21 (1973) 571–574.

[63] H. Moulinec, P. Suquet, A numerical method for computing the overall response of nonlinear composites with complex microstructure, Computer methods in applied mechanics and engineering 157 (1998) 69–94.

[64] A. Fritsch, C. Hellmich, 'universal' microstructural patterns in cortical and trabecular, extracellular and extravascular bone materials: Micromechanics-based prediction of anisotropic elasticity, Journal of Theoretical Biology 244 (2007) 597–620.

[65] J. M. Deuerling, W. Yue, A. A. E. Orías, R. K. Roeder, Specimen-specific multi-scale model for the anisotropic elastic constants of human cortical bone, Journal of biomechanics 42 (2009) 2061–2067.

[66] Y. Bala, B. Depalle, T. Douillard, S. Meille, P. Clément, H. Follet, J. Chevalier, G. Boivin, Respective roles of organic and mineral components of human cortical bone matrix in micromechanical behavior: an instrumented indentation study, Journal of the mechanical behavior of biomedical materials 4 (2011) 1473–1482.

[67] K. Raum, R. O. Cleveland, F. Peyrin, P. Laugier, Derivation of elastic stiffness from site-matched mineral density and acoustic impedance maps, Physics in medicine and biology 51 (2006) 747.

[68] X. Cai, R. Brenner, L. Peralta, C. Olivier, P.-J. Gouttenoire, F. Peyrin, D. Cassereau, P. Laugier, Q. Grimal, Homogenization of cortical bone reveals that the organization and shape of pores marginally affect elasticity (accepted), Journal of the Royal Society Interface (2019).

[69] D. J. Rudy, J. M. Deuerling, A. A. E. Orías, R. K. Roeder, Anatomic variation in the elastic inhomogeneity and anisotropy of human femoral cortical bone tissue is consistent across multiple donors, Journal of biomechanics 44 (2011) 1817–1820.

[70] I. S. Hage, R. F. Hamade, Intracortical stiffness of mid-diaphysis femur bovine bone: lacunar-canalicular based homogenization numerical solutions and microhardness measurements., Journal of materials science. Materials in medicine 28 (2017) 135.

[71] A. Boskey, Bone mineral crystal size, Osteoporosis International 14 Suppl 5 (2003) S16–20; discussion S20–1.

[72] M. Granke, A. Gourrier, F. Rupin, K. Raum, F. Peyrin, M. Burghammer, A. Saïed, P. Laugier, Microfibril orientation dominates the microelastic properties of human bone tissue at the lamellar length scale, PLoS One 8 (2013) e58043.

[73] S. Schrof, P. Varga, B. Hesse, M. Schöne, R. Schütz, A. Masic, K. Raum, Multimodal correlative investigation of the interplaying micro-architecture, chemical composition and mechanical properties of human cortical bone tissue reveals predominant role of fibrillar organization in determining microelastic tissue properties, Acta Biomaterialia 44 (2016) 51–64.

[74] M. Granke, M. D. Does, J. S. Nyman, The role of water compartments in the material properties of cortical bone, Calcified Tissue International 97 (2015) 292–307.

[75] P. Dong, S. Haupert, B. Hesse, M. Langer, P.-J. Gouttenoire, V. Bousson, F. Peyrin, 3d osteocyte lacunar morphometric properties and distributions in human femoral cortical bone using synchrotron radiation micro-ct images, Bone 60 (2014) 172–185.

[76] B. Yu, M. Langer, A. Pacureanu, R. Gauthier, H. Follet, D. Mitton, C. Olivier, P. Cloetens, F. Peyrin, Assessment of imaging quality in magnified phase ct of human bone tissue at the nanoscale, 2017.

[77] E. Lefèvre, P. Lasaygues, C. Baron, C. Payan, F. Launay, H. Follet, M. Pithioux, Analyzing the anisotropic hooke's law for children's cortical bone, Journal of the mechanical behavior of biomedical materials 49 (2015) 370–377.

[78] X. Cai, R. Brenner, P. Laugier, Q. Grimal, Cortical bone matrix anisotropic stiffness determined by inverse homogenization and resonant ultrasound spectroscopy, in: 8th World Congress of Biomechanics, 2018.

[79] A. Migliori, J. L. Sarrao, Resonant Ultrasound Spectroscopy, Wiley, New York, 1997.

[80] S. Bernard, Q. Grimal, P. Laugier, Resonant ultrasound spectroscopy for viscoelastic characterization of anisotropic attenuative solid materials, The Journal of the Acoustical Society of America 135 (2014) 2601–2613.

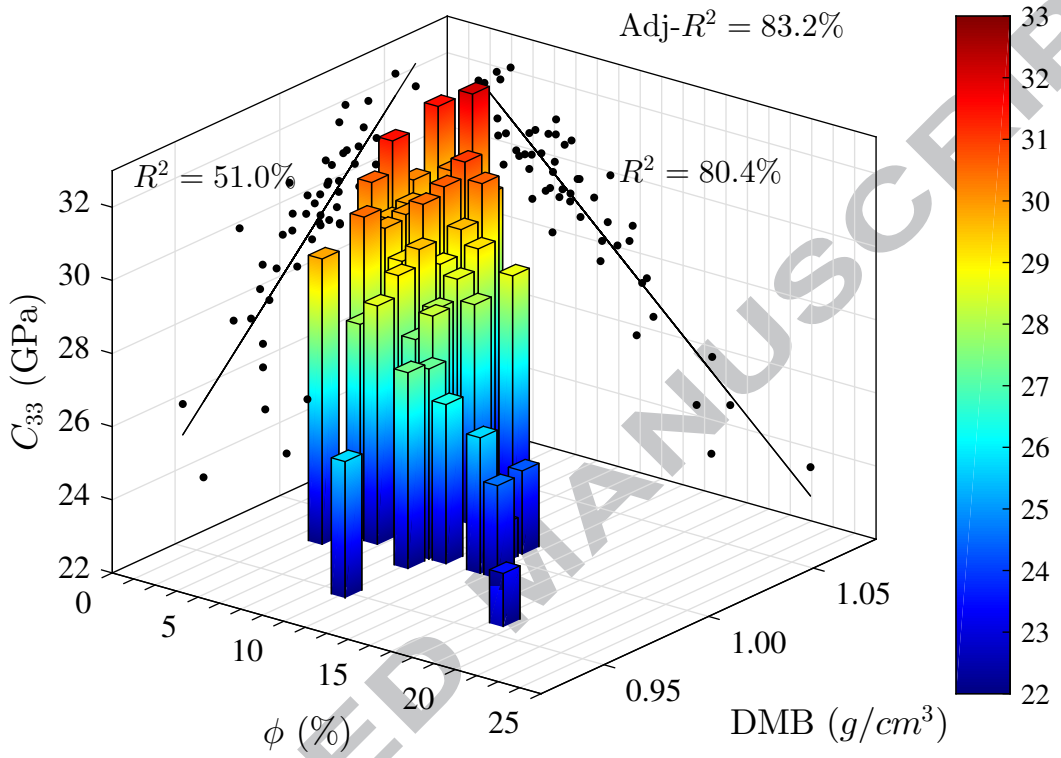

Statement of significance

This study reports the relationships between microstructure, composition and the mesoscale anisotropic elastic properties of human femoral cortical bone in elderly. For the first time, we provide data covering the complete anisotropic elastic tensor, the microstructure of cortical vascular porosity, mineral and collagen characteristics obtained from the same or adjacent samples in each donor. The results revealed that cortical vascular porosity and degree of mineralization of bone are the most important determinants of bone anisotropic stiffness at the mesoscale. The presented data gives strong experimental evidence and basis for further development of biomechanical models for human cortical bone.